Atmos. Chem. Phys., 7, 1471–1489, 2007
www.atmos-chem-phys.net/7/1471/2007/

Atmospheric Chemistry and Physics

Mesoscale modelling of water vapour in the tropical UTLS: two case studies from the HIBISCUS campaign

V. Marécal[1], G. Durry[2,3], K. Longo[4], S. Freitas[4], E. D. Rivière[2], and M. Pirre[1]

[1]Laboratoire de Physique et Chimie de l'Environnement, CNRS and Université d'Orléans, 3A Avenue de la Recherche Scientifique, 45071 Orléans cedex 2, France
[2]Groupe de Spectroscopie Moléculaire et Atmosphérique, CNRS and Université de Reims, Moulin de la Housse, B.P. 1039, 51687 Reims Cedex, France
[3]Service d'Aéronomie, CNRS and Institut Pierre Simon Laplace, 91371 Verrières-le-Buisson Cedex, France
[4]Centro de Previsão de Tempo e Estudos Climàticos, Rodovia Presidente Dutra, km 40 SPRJ 12630-000, Cachoeira Paulista – SP, Brazil

Received: 12 May 2006 – Published in Atmos. Chem. Phys. Discuss.: 29 August 2006
Revised: 20 November 2006 – Accepted: 28 February 2007 – Published: 19 March 2007

Abstract. In this study, we evaluate the ability of the BRAMS (Brazilian Regional Atmospheric Modeling System) mesoscale model compared to ECMWF global analysis to simulate the observed vertical variations of water vapour in the tropical upper troposphere and lower stratosphere (UTLS). The observations are balloon-borne measurements of water vapour mixing ratio and temperature from micro-SDLA (Tunable Diode Laser Spectrometer) instrument. Data from two balloon flights performed during the 2004 HIBISCUS field campaign are used to compare with the mesoscale simulations and to the ECMWF analysis.

The observations exhibit fine scale vertical structures of water vapour of a few hundred meters height. The ECMWF vertical resolution ($\sim$1 km) is too coarse to capture these vertical structures in the UTLS. With a vertical resolution similar to ECMWF, the mesoscale model performs better than ECMWF analysis for water vapour in the upper troposphere and similarly or slightly worse for temperature. The BRAMS model with 250 m vertical resolution is able to capture more of the observed fine scale vertical variations of water vapour compared to runs with a coarser vertical resolution. This is mainly related to: (i) the enhanced vertical resolution in the UTLS and (ii) to the more detailed microphysical parameterization providing ice supersaturations as in the observations. In near saturated or supersaturated layers, the mesoscale model predicted relative humidity with respect to ice saturation is close to observations provided that the temperature profile is realistic. For temperature, the ECMWF analysis gives good results partly attributed to data assimilation. The analysis of the mesoscale model results showed that the vertical variations of the water vapour profile depends on the dynamics in unsaturated layer while the microphysical processes play a major role in saturated/supersaturated layers.

In the lower stratosphere, the ECMWF model and the BRAMS model give very similar water vapour profiles that are significantly drier than micro-SDLA measurements. This similarity comes from the fact that BRAMS is initialised using ECMWF analysis and that no mesoscale process acts in the stratosphere leading to no modification of the BRAMS results with respect to ECMWF analysis.

Correspondence to: V. Marécal
(virginie.marecal@cnrs-orleans.fr)

1 Introduction

It is known that the stratosphere is dry since Brewer (1949) who performed water vapour measurements with a balloon-borne frost-point hygrometer in England. This rather late discovery concerning a major air compound is related to the technical difficulty of measuring very low water vapour mixing ratios down to a few ppmv at low temperatures. In the low and mid-troposphere, humidity is operationally monitored through the radio-sounding network providing fairly accurate in situ measurements of water vapour with a fine vertical resolution. In the upper troposphere and the lower stratosphere (UTLS), it is known that the radio-sounding sensors generally used for measuring humidity are not reliable because of the low temperature conditions. This is even more critical in the tropics where temperatures down to about -80°C are generally found around the tropopause.

Published by Copernicus GmbH on behalf of the European Geosciences Union.

Miloshevich et al. (2001), Fujiwara et al. (2003) and Turner et al. (2003) showed that the Vailsala RS80 radiosonde system, which is the most widely used, has a dry bias that increases with decreasing temperatures. Newer sondes (Vaisala RS90) that are fitted with a different humidity sensor are designed to provide more accurate humidity measurements at cold temperatures for the future operational network. The current operational monitoring from radiosondes is complemented by remote sensing observations from satellite instruments, mainly vertical and limb sounders, that provide a global coverage but with much coarser vertical and horizontal resolutions than radiosondes. Therefore, remote sensing observations do not allow the study of the fine scale processes affecting the vertical structure of the water vapour field within the UTLS.

On the research side, chiefly three types of instruments flown on aircraft or balloon platforms have proven their ability to provide in situ water vapour measurements in the UTLS with an accuracy within a few percents: Lyman-α hygrometers (e.g. Hintsa et al., 1999; Zöger et al., 1999), frost-point hygrometers (e.g. Ovarlez and Van Velthoven, 1997) and tunable diode laser spectrometers (e.g. May, 1998; Durry and Mégie 1999). The measurements obtained from these instruments showed a large vertical variability of the water vapour mixing ratio in the UTLS and also significant differences between the measurements gathered at different latitudes and seasons (e.g. Ovarlez et al., 2000; Vömel et al., 2002; Offermann et al., 2002; Durry et al., 2002; Durry and Hauchecorne, 2005). The water vapour variability in the UTLS is related to the history of the air mass sampled at a given level that can be affected by both dynamical (long-range horizontal transport, vertical transport by convection, stratosphere-troposphere exchanges) and microphysical processes (mainly dehydration by ice nucleation, subsequent growth and sedimentation of the condensed particles). The understanding and the prediction of the water vapour distribution in the tropical upper troposphere is currently a key issue since this region is likely to control the entry of water vapour in the stratosphere (e.g. Holton et al., 1995; Hatsushika and Yamazaki, 2003; Fueglistaler et al., 2004).

The measurements available so far are not sufficient to provide a full picture of the relative impact of the different processes affecting the water vapour distribution in the tropics. The modelling approach can be used to complement these observations, in particular three-dimensional meteorological models that represent in a consistent manner the dynamical and microphysical processes affecting the water distribution. Global meteorological models, such as the ECMWF model, do not generally use a vertical resolution fine enough in the UTLS to resolve the observed small scale variability of humidity. Moreover, the parameterizations mostly used in global models only include a limited number of microphysical processes. To overcome these weaknesses, a possible approach is to use a Lagrangian one-dimensional microphysical model along trajectories extracted from global analyses (Gettelman et al., 2002; Jensen and Pfister, 2004). Trajectories are generally interpolated from 4-daily analyses missing short-time or local variations of temperature that can impact on the microphysics. An alternative tool is the three-dimensional limited-area meteorological model, also called a mesoscale model, that can be run with a fine vertical resolution in the UTLS and that can account for a large number of microphysical processes. The time evolution of the microphysics being calculated at each model time step, the microphysics is always fully consistent with the model dynamics and thermodynamics. These models and their associated parameterizations are designed to provide realistic forecasts of tropospheric weather phenomena. However, cirrus occurring in the uppermost troposphere or lower stratosphere may not be well represented in mesoscale models. These models commonly use a microphysical parameterization of bulk type in which only one type of small ice crystals is represented, whereas in reality, cirrus are composed of a large variety of ice crystals. Moreover, they rely on global analyses for initial and boundary conditions that may be uncertain in the UTLS since few humidity observations are available for assimilation systems in this atmospheric layer.

In this context, the objective of this paper is to evaluate the potential benefit of using a mesoscale model compared to a global analysis to reproduce the vertical variations of water vapour in the tropical UTLS. For this purpose the temperature and water vapour profiles from mesoscale model simulations and from ECMWF analyses were compared to the measurements gathered by the micro-SDLA instrument during the balloon flights SF2 and SF4 launched in the framework of the field campaign of the HIBISCUS project (Impact of tropical convection on the upper troposphere and lower stratosphere at global scale). These two flights were performed in different meteorological conditions: SF2 ahead of a cold front event and SF4 nearby a strong convective system. HIBISCUS was a European funded project aiming at studying the air composition of the tropical UTLS and in particular its link with the tropical convection. The main HIBISCUS field campaign took place during the wet season in February and March 2004 in Bauru (State of Saõ Paulo in Brazil). This campaign was mainly based on balloon-borne measurements of chemical species and water vapour and complemented by modelling studies (Pommereau et al., 2007). Durry et al. (2006) interpreted SF2 and SF4 water vapour data using complementary observations of ozone and CH_4. The present paper is a complementary study focused on the simulation of the water vapour distribution in the UTLS by a mesoscale model.

In Sect. 2, the micro-SDLA instrument is described. A brief description of the BRAMS mesoscale model used in this study and of the ECMWF model is given in Sect. 3. SF2 (resp. SF4) measurements and the corresponding modelling results are discussed in Sect. 4 (resp. Sect. 5). The conclusions are given in Sect. 6.

2 Description of Micro-SDLA instrument

The micro-SDLA sensor is a balloon borne near-infrared diode laser spectrometer that yields in situ measurements of H_2O, CH_4 and CO_2 in the UTLS by absorption spectroscopy (description found in Durry et al., 2004). Three InGaAs laser diodes emitting respectively at 1.39 μm (H_2O), 1.60 μm (CO_2) and 1.65 μm (CH_4) are connected with optical fibers to a multipass optical cell operated open to the atmosphere that provides a 28 m absorption path length. The laser beams are absorbed in situ by the ambient molecules as it is propagated between both mirrors of the optical cell and in situ absorption spectra are recorded at the cell output using a direct-differential detection technique. The amount of absorbed laser energy is then related to the molecular concentration using the Beer-Lambert Law, in situ pressure and temperature measurements and an adequate molecular model (Durry and Megie, 1999). The atmospheric pressure is obtained from an onboard Paroscientific Inc baratron gauge with an accuracy of ~0.01 hPa. Three meteorological thermistors (VIZ Manufacturing Company) located at different places in the gondola, are used to measure in situ the temperature with a precision of 1 K. Regarding water vapor, the instrument provides a dynamical range for the measurements of four orders of magnitude that permits to measure continuously H_2O in the troposphere and the lower stratosphere despite the large difference in the H_2O amounts observed in both regions of the atmosphere (Durry and Megie, 2000). For the flights discussed in this paper, the temporal resolution was of one H_2O concentration sample per second for SF2 and was upgraded to four samples per second for the second flight, SF4. The H_2O molecular mixing ratio was retrieved from the absorption spectra with a non-linear least-squares fit to the full molecular line shape and by using our set of revisited molecular parameters, i.e. H_2O line strengths and pressure-broadening coefficients from Parvitte et al. (2002) and Durry et al. (2005). The measurement error in the H_2O concentration ranges from 5% to 10%. A complete description of the retrieval process and associate sources of errors is found in Durry and Megie (1999) and Durry et al. (2002). For HIBISCUS, the micro-SDLA was operated in an unattended manner without telemetry- telecommand from small open balloons inflated with 3000 $m^3$of Helium to probe the troposphere and the lower stratosphere. The spectra were stored onboard and processed after the flights. The reported H_2O data gathered in the UTLS, were recorded as usual at nighttimes during the slow descent of the gondola to prevent pollution of the measurement by water vapor outgassing from the balloon envelope (Durry and Megie, 2000; Durry et al., 2004). The H_2O data in the mid-troposphere were obtained under parachutes after cut-off from the flight chain (Durry et al., 2004).

3 Modelling tools

3.1 Mesoscale model and simulation setup

The regional model used in this study is the BRAMS (Brazilian Regional Atmospheric Modeling System, http://www.cptec.inpe.br/brams). BRAMS is a new version of the RAMS (Walko et al., 2000) tailored to the tropics. The BRAMS/RAMS model is a multipurpose numerical prediction model designed to simulate atmospheric circulations spanning in scale from hemispheric scales down to large eddy simulations of the planetary boundary layer. Among the additional possibilities of BRAMS compared to RAMS version 5.04 are the ensemble version of shallow cumulus and deep convection parameterizations (Grell and Devenyi, 2002; Freitas et al., 2005), new 1 km vegetation data for South America, heterogeneous soil moisture assimilation procedure (Gevaerd and Freitas, 2006) and SIB2.5 surface parameterization. The parameterization used for longwave/shortwave radiation is from Harrington (1997). It is a two-stream scheme which interacts with liquid and ice hydrometeor size spectra. The cloud microphysics is the single moment bulk scheme from Walko et al. (1995) which includes five categories of ice: pristine ice crystals, snow, aggregates, graupel and hail. The turbulence parametrization is from the Mellor and Yamada (1982) level 2.5 scheme which employs a prognostic turbulent kinetic energy.

A BRAMS simulation was performed for each flight in order to analyse the model ability to simulate the observed temperature and water vapour profiles (called reference simulation hereafter). The reference simulation for both flights is similar except for the initial time/date of the simulation. The simulation starts on 12 February 2004 at 00:00 UTC for SF2 and on 23 February 2004 at 00:00 UTC for SF4 and lasts 60 h for both flights. The reference run includes one grid centred on Bauru. The domain dimension is 2800×2400 km^2 (see domain plotted in Fig. 2) and is chosen to include the large scale dynamic fluxes that can possibly affect the water vapour profiles for both flights. Because of the fairly large domain extension we chose 20 km horizontal grid-spacing. The vertical coordinate is a terrain-following height coordinate extending from the surface to 30 km altitude with a 250 m grid-spacing between 13 and 20 km altitude (total number of levels=74). The initial conditions are from the ECMWF operational analysis. The BRAMS fields are constrained at the boundaries by Newtonian relaxation (nudging) with the 6-hourly ECMWF operational analyses. The initial soil moisture is derived from the assimilation of TRMM accumulated rainfall estimates (Gevaerd and Freitas, 2006). The paramaterizations of sub-grid scale shallow and deep convection are used (Grell and Devenyi, 2002; Freitas et al., 2005).

Backward trajectories were calculated from the model outputs along the balloon track locations using the methodology proposed by Freitas et al. (2000) which takes into account the subgrid effects of wet convective processes. The

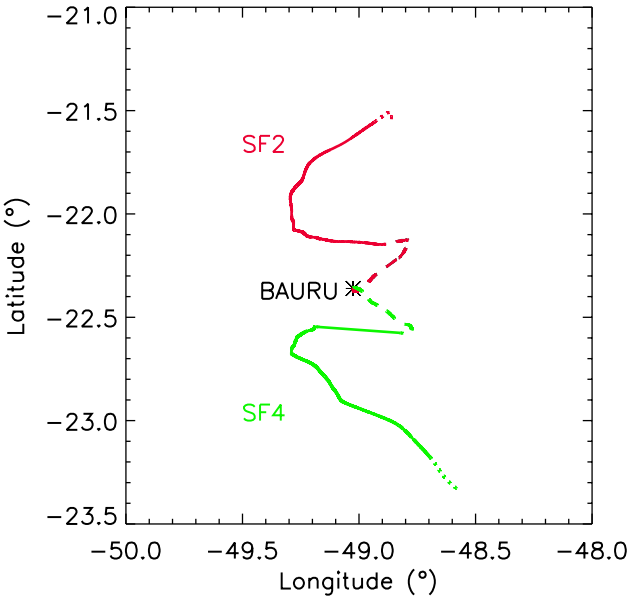

Fig. 1. Projection on the horizontal plan of the trajectory of the SF2 and SF4 balloon flights. The dashed, solid and dotted lines correspond respectively to the ascent, slow descent and rapid descent after cut down of the balloon. The red lines correspond to SF2 and green lines to SF4.

trajectories determined by this method are reliable providing that the modelled convective precipitation is well located.

Four sensitivity simulations were also run to test the impact on the results of the horizontal and vertical resolutions and of the microphysical scheme. The setup of theses simulations is explained in Sects. 4 and 5 together with the corresponding analysis of the results.

3.2 ECMWF analysis

The operational global analysis produced at ECMWF (European Centre for Medium-range Weather Forecasts) are used in this study. One major characteristic of these analyses is that it includes the stratosphere up to the 1 hPa level. At the date of the HIBISCUS campaign, the ECMWF model had 60 vertical levels and a T511 truncation. ECMWF fields used are extracted on a $0.5° \times 0.5°$ grid. The assimilation system is a four-dimensional variational system including data over 12 h windows. For humidity, the data assimilated are the specific humidity profiles from radiosondes below 300 hPa, surface relative humidity and satellite radiances including moisture sensitivity. The longwave radiation parametrization (Morcrette et al., 1998) is based on the Rapid Radiation Transfer Model (Mlawer et al., 1997). It includes cloud effects using maximum-random overlap of effective cloud layers. The shortwave radiation scheme was originally developed by Fouquart and Bonnel (1980) and revised by Morcrette (1993). It takes into account the cloud properties for ice and liquid clouds.

4 Results for SF2 flight

4.1 SF2 flight and its meteorological environment

The SF2 balloon was launched from Bauru, State of São Paulo, Brazil (22.36° S, 49.02° W) at 20:18 UTC (18:18 local summer time) on 13 February 2004. The balloon reached a maximum altitude of 20 km at sunset (22:11 UTC). Then the balloon experienced 3 h of slow night time descent down to 11.8 km where it was cut down. The trajectory of the balloon is shown in Fig. 1.

On 13 February 2004, the western and central parts of the State of São Paulo were located within the warm-sector ahead of a cold front advancing from Argentina, which reached South Brazil during the afternoon. During the afternoon of 13 February 2004, the Bauru radar observations showed that there was a moderate convective activity around Bauru with several weak convective cells developing within the radar range (240 km). At the time of the launch, there was a large area of instability moving in from north-west and west, but that never came closer than 300 km from the balloon track. It only reached Bauru around 07:00 UTC on 14 February, long after the end of the balloon flight. The meteorological situation is illustrated in Fig. 2a from the accumulated rainfall estimated by the Tropical Rainfall Measuring Mission (TRMM, http://trmm.gsfc.nasa.gov) between 19:30 UTC on 13 February and 10:30 UTC on 14 February. More details on the meteorological situation can be found in Durry et al. (2006).

4.2 SF2 water vapour and temperature profiles

For the SF2 flight analysis, we make use of the H_2O data yielded by the micro-SDLA in the altitude region ranging from 18.5 km altitude after sunset (22:45 UTC) down to 4.6 km altitude (00:46 UTC) during its descent.

The water vapour mixing ratio (noted r_v hereafter) and the temperature profiles from micro-SDLA are shown in Figs. 3a and b. Note that there were no data between 12.774 and 13.385 km altitude because of technical problems. The water vapour profile (Fig. 3a) shows a large variability below 10 km altitude with a dry layer between 5 and 7 km. Above 10 km, there is a decrease with altitude up to an hygropause at 17 km altitude reaching ∼3 ppmv with enhanced variability between 14 and 17 km. Above 17 km, r_v slowly increases with altitude. The temperature (Fig. 3b) decreases with altitude up to the cold point tropopause (−78.8°C) at 15.5 km altitude. Above 15.5 km, there is a large variability of the temperature profile with a tendency to slowly increase with altitude. Figure 3c depicts the relative humidity with respect to ice saturation in % (RHI) calculated from the measured temperatures and r_v. To allow a fair comparison with the model results (Sect. 5), the calculation of RHI is based on the formula of the saturation pressure with respect to ice used in the BRAMS model (Flatau et al., 1992) which provides

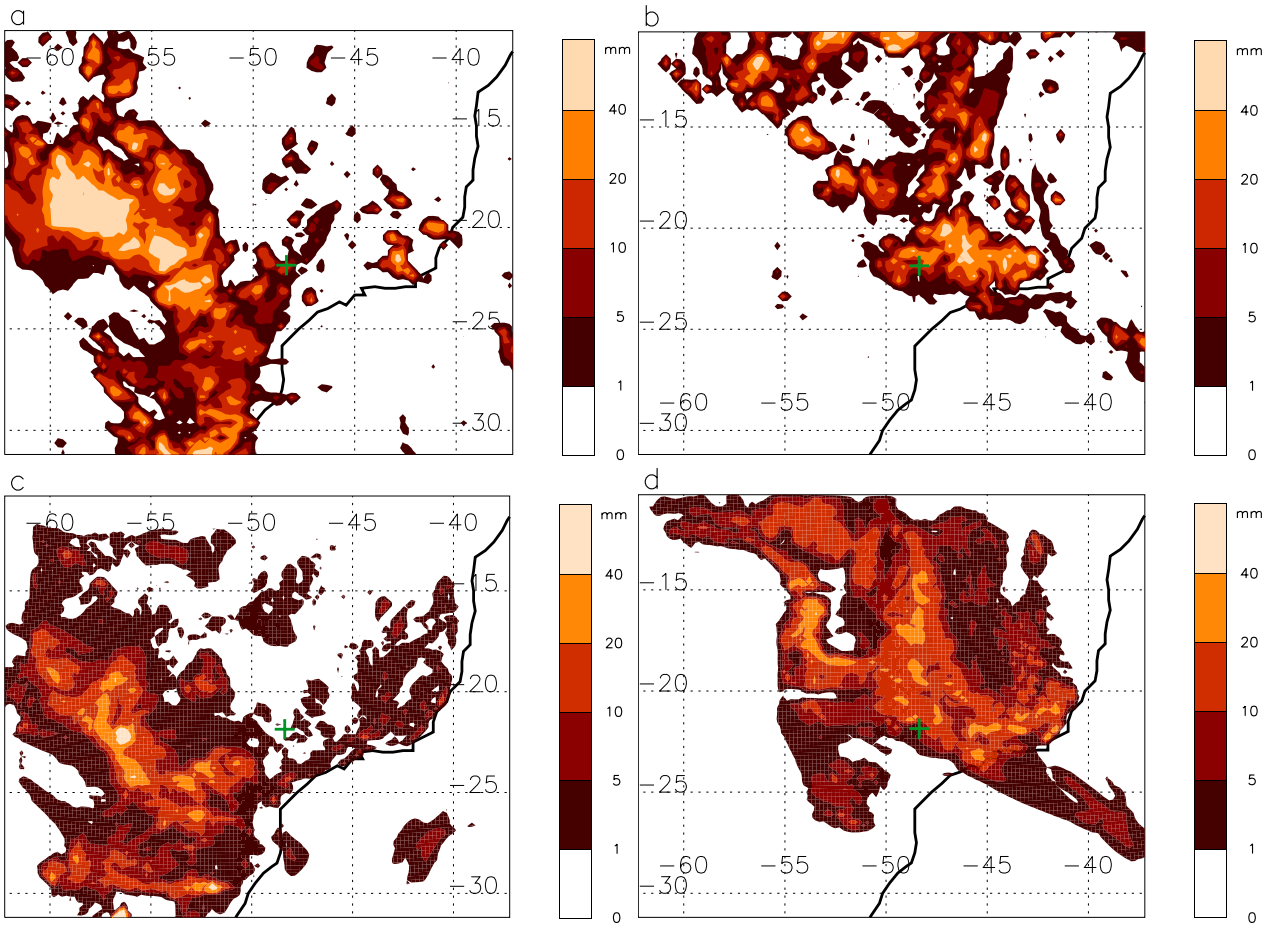

Fig. 2. Accumulated rainfall in mm **(a)** from TRMM between 19:30 UTC on 13 February 2004 and 10:30 UTC on 14 February 2004, **(b)** from TRMM between 16:30 UTC on 24 February 2004 and 04:30 UTC on 25 February 2004, **(c)** from the reference run between 19:30 UTC on 13 February 2004 and 10:30 UTC on 14 February 2004, **(d)** from the reference run between 16:30 UTC on 24 February 2004 and 04:30 UTC on 25 February 2004. The green cross corresponds to the location of Bauru balloon launch site. The area plotted in these figures corresponds to the domain used in the BRAMS simulations.

RHI values close within +/−0.5% to those found using Sontag (1998)'s formula. The RHI profile shows that the air is very close to saturation or supersaturated between 10 and 16 km altitude. The very large supersaturation values up to RHI=190% are consistent with the water vapour data presented in Ovarlez et al. (2000), Ovarlez et al. (2002) and Jensen et al. (2005a, b). The two layers where very large super-saturations occur (around 13.5 and around 15.5 km altitude) are associated with enhanced water vapour mixing ratios. This indicates that, in these layers, the excess of water vapour has not been removed yet at the time of the measurements by ice nucleation and subsequent sedimentation of the condensed particles. Nevertheless, there are favourable conditions for the air to dehydrate within the following hours.

4.3 Comparison of the reference run and ECMWF analysis with SF2 measurements

The comparison between micro-SDLA SF2 measurements and the ECMWF analysis is shown in Fig. 4 and the comparison between micro-SDLA SF2 measurements and the BRAMS reference run is shown in Fig. 5. The micro-SDLA data are averaged vertically in Fig. 4 (resp. Fig. 5) to match the ECMWF (resp. BRAMS reference run) vertical grid. To plot the ECMWF results, we have selected the profile the closest to the SF2 descent mean location plus the 8 profiles around from the 14 February 00:00 UTC analysis fields. To plot the BRAMS reference simulation results, we have selected the profile closest to the SF2 descent mean location plus all the profiles around as far as 60 km from this profile from hourly outputs between 22:00 UTC on 13 February 2004 and 01:00 UTC on 14 February 2004. This time

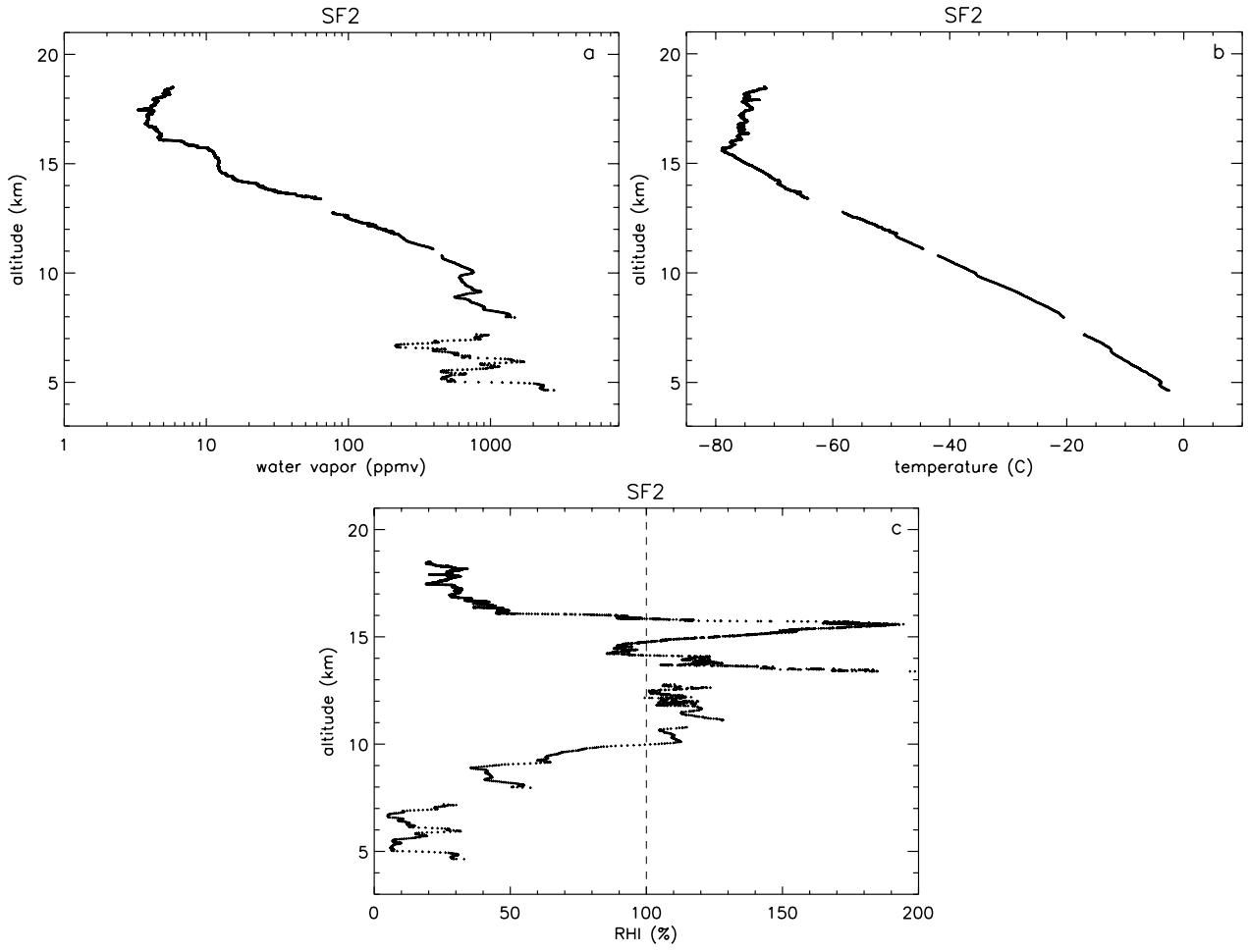

Fig. 3. SF2 flight: **(a)** water vapour mixing ratio in ppmv from micro-SDLA measurements, **(b)** temperature in °C from micro-SDLA measurements, **(c)** derived relative humidity with respect to ice saturation (RHI) in %.

interval corresponds approximately to the descent duration. Note that in the 13–20 km layer where the BRAMS vertical resolution is 250 m (29 levels), there are only 8 ECMWF model levels corresponding to ∼1 km vertical spacing. Statistical results comparing model and observations are given in Table 1. For the statistical analysis, RHI results were preferred to r_v results to evaluate the water vapour model performance since r_v values cover several orders of magnitude and therefore statistics for r_v would be weighted towards the large r_v at low altitudes. The other reason for this choice is that RHI gives not only information on the water vapour but also on the state of the air parcel with respect to sub/supersaturation. The correlation for temperature is not given since it is greater than 0.999 for all model configurations.

Figures 4 and 5 show that the main water vapour and temperature features observed by micro-SDLA in the UTLS are largely smoothed when averaged on the ECMWF vertical grid while they are still present when averaged on the BRAMS reference run grid. ECMWF analysis does not reproduce the observed variations in the UTLS. This is related to the vertical resolution which only allows the simulation of structures having a vertical extension greater than a few kilometres. Below 10 km, the ECMWF analysis exhibits a dry layer but moister than the mean microSDLA profile below 8 km. From 12 km upwards, ECMWF analysis generally underestimates r_v, particularly above 15 km altitude. The dry bias of the ECMWF analysis in the upper troposphere was already pointed out in several studies (e.g. Ovarlez and Van Velthoven, 1997; Ovarlez et al., 2000; Spichtinger et al., 2005). In the stratosphere, the ECMWF water vapour analysis field is nearly constant since no humidity data are available for assimilation. For the temperature (Fig. 4b), there is a generally good agreement between micro-SDLA and the ECMWF analysis within 2 K. In particular, the ECMWF analysis exhibits a well-defined minimum of temperature at the cold point tropopause similar to micro-SDLA. In Fig. 4c, the ECMWF RHI profile shape is qualitatively similar to observations as illustrated by a RHI correlation of 0.905.

Table 1. Statistical results for SF2 flight: correlation and RMSE (Root Mean Square Error) between the model (ECMWF or BRAMS) and micro-SDLA averaged over the corresponding model grid.

	temperature RMSE (K)	RHI correlation	RHI RMSE (%)
ECMWF analysis	1.69	0.905	26.5
ECMWF 48h forecast started on 12 Feb 2004 at 00:00 UTC	1.84	0.827	36.4
Run with 1 km vertical resolution	1.60	0.937	16.4
Reference run	1.76	0.850	26.0
Run with 50 km horizontal resolution	1.72	0.839	26.1
Run with 5 km resolution (2 grids)	1.84	0.842	26.9
Run with simplified microphysics	1.85	0.767	34.6

Quantitatively, the ECMWF RHI is close to the observations mainly below 10 km leading to 26.5% for the RMSE value. Note that there are no ECMWF RHI values greater than 100%. This illustrates the fact that supersaturated states with respect to ice are not allowed below a temperature of -23°C in the ECMWF model. Therefore, it is not possible in the ECMWF analysis to reproduce the observed supersaturated layers in the UTLS. Moreover, because water vapour is removed instantaneously as condensed water below -23°C when superstaurated with respect to ice, the ECMWF analysis generally underestimates r_v compared to observations.

To make a fair comparison between results of the ECMWF analysis and of the BRAMS model, a sensitivity simulation was performed with a 1 km vertical resolution in the UTLS ($\sim$ ECMWF vertical resolution) instead of the 250 m resolution in the reference run. In Table 1 the statistical results for the 1 km-resolution BRAMS simulation are calculated using the micro-SDLA data averaged over the BRAMS 1km vertical grid. Results in Table 1 show that the sensitivity run provides results for temperature similar to ECMWF analysis and a RHI mean profile (RHI RMSE=16.4%) significantly closer to the observations than ECMWF analysis (RHI RMSE=26.5%). This means that with a similar vertical resolution BRAMS performs similarly to ECMWF analysis for temperature but significantly better for water vapour. Note that it is not pertinent to compare the statistics of the ECMWF analysis to those of the reference run since the former (i) are calculated over a smaller number of points because of the different vertical grid spacing used and (ii) correspond to an averaged profile in which the small scale structures are largely smoothed.

As shown in Fig. 5, the vertical variations of r_v, temperature and RHI are generally reproduced in the BRAMS simulation although smoothed compared to the micro-SDLA measurements. The reference simulation provides the dry layer below 10 km altitude but not as dry as in the observations, similarly to the ECMWF analysis. In this altitude range, the SF2 balloon was flown in a transition region between a dry and a moist air mass where the water vapour gradient is strong. The difference between the model and the observations indicates that the model dynamics has driven slightly too early the moist air mass associated to the front towards the Bauru area. The zigzag shape found in the observations in this layer is also not reproduced by the mesoscale model. The small scale vertical variations in the observations are likely due to sub-grid isolated convective cells captured by the measurements but not by the model because of its spatial resolution. This hypothesis is supported by the fact that the backward trajectories crossed an area in which there were several small convective cells of a few kilometres horizontal extension in the Bauru radar observations. In the 10–14 km layer, the reference run shows a very good agreement with micro-SDLA measurements. In the 14–17.3 km range, the S-shape of the mean micro-SDLA profile is reproduced by the model but with less pronounced minima. Above 17.5 km altitude, the model gives nearly constant values for r_v with a low variability between the selected profiles as in ECMWF analysis. For temperature (see Fig. 5b), the reference simulation is generally in good agreement with the measurements (RMSE=1.76 K) except near the cold point tropopause level where the local sharp minimum is not simulated by the model. There is a $\sim$5 K difference at 15.5 km altitude. As shown in Fig. 4b, this minimum is present in the ECMWF analysis. This important feature does not appear in the ECMWF 48 h forecast started on 12 February at 00:00 UTC. It is brought in the 14 February 00:00 UTC analysis by the assimilation of observations. This indicates that the precursor information leading to this feature was not present in the 12 February 00:00 UTC ECMWF analysis used as initial state for the BRAMS simulations. More generally, the analysis gives better statistics than the forecast (see Table 1) thanks to data assimilation.

The general shape of the observed RHI profile in Fig. 5c is reproduced by the model (RHI correlation = 0.850 and RHI RMSE=26.0%) except around 15.5 km and 13.5 km altitude where the model does not provide the observed large

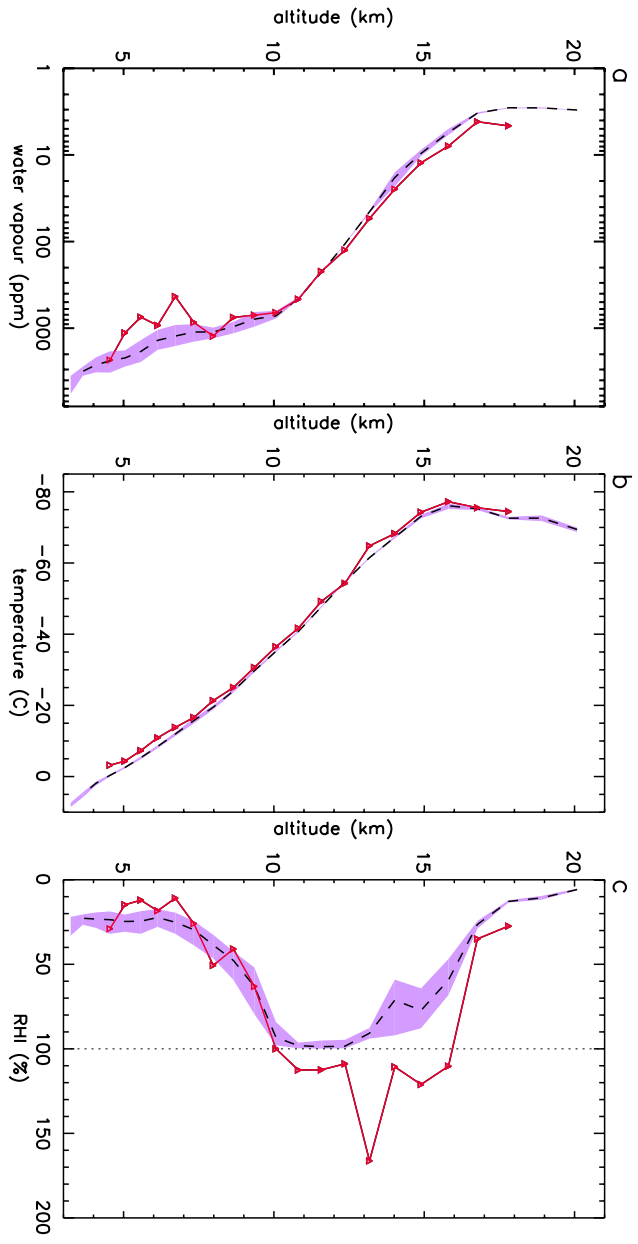

Fig. 4. Comparison between ECMWF analysis and micro-SDLA SF2 measurements **(a)** for water vapour in ppmv, **(b)** for temperature in °C and **(c)** for RHI in %. The micro-SDLA data are averaged on the ECMWF model vertical grid and shown as a solid red line with the triangles showing the model levels. The black dashed line and the purple area show, respectively, the mean and the minimum/maximum for a set of selected model profiles. Details on the selected profiles are given in the text.

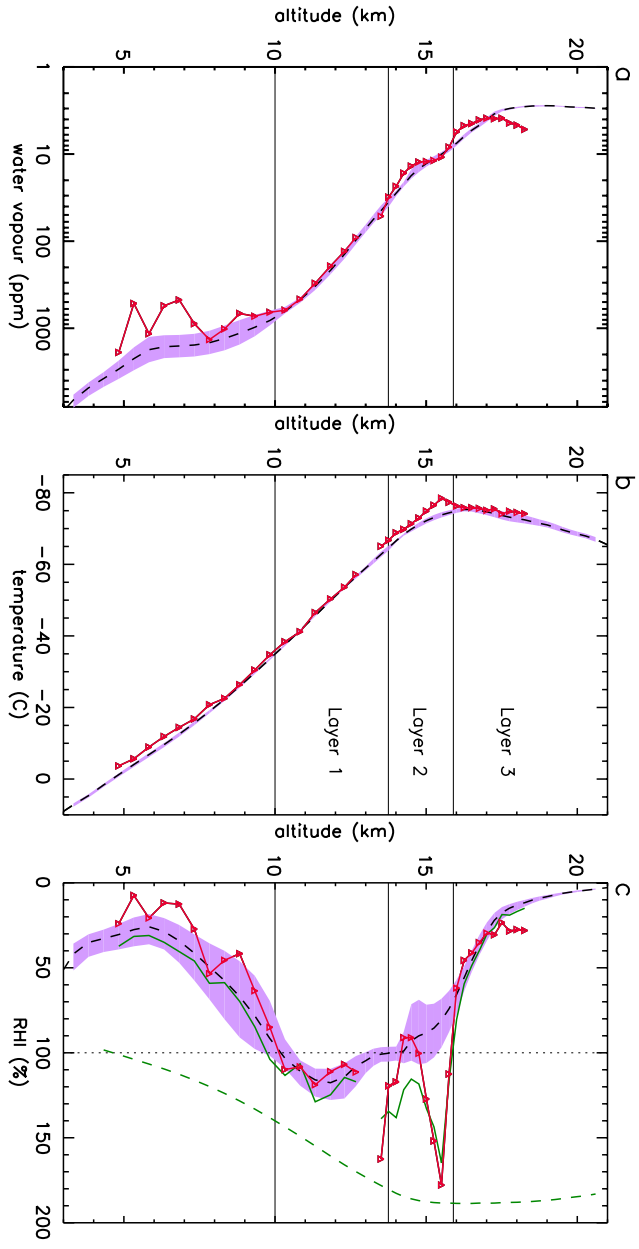

Fig. 5. Comparison between BRAMS reference simulation and micro-SDLA SF2 measurements **(a)** for water vapour in ppmv, **(b)** for temperature in °C and **(c)** for RHI in %. The micro-SDLA data are averaged on the BRAMS model vertical grid and shown as a solid red line with the triangles showing the model levels. The black dashed line and the purple area show, respectively, the mean and the minimum/maximum for a set of selected model profiles. Details on the selected profiles are given in the text. In (c), the green solid line corresponds to RHI calculated using r_v from the BRAMS reference run and the micro-SDLA temperature. The green dashed line corresponds to 100% saturation with respect to liquid water calculated using BRAMS mean temperature profile.

supersaturations and above 17.3 km where the model is significantly dryer. Unlike ECMWF analysis, BRAMS microphysical scheme allows supersaturations with respect to ice at a given temperature. The threshold for the ice supersaturation in the model is 100% for the relative humidity with respect to liquid water. This assumption is related to the BRAMS microphysical parameterization in which cloud

water mixing ratio is diagnosed using a test based on the saturation with respect to liquid water and the prognostic mixing ratios of total water, rain, cloud ice, aggregates, snow, graupel and hail (Walko et al., 1995). For the tropical UTLS conditions, this constraint (100% relative humidity with respect to liquid water) leads to large possible model ice supersaturations as illustrated in Fig. 5c (green dashed line). This means that the observed large ice supersaturations can be simulated by BRAMS leading to a slower removal of water vapour by ice nucleation than in the ECMWF model. This is illustrated by the generally greater values of r_v simulated by BRAMS in the 12–17 km layer compared to the ECMWF analysis leading to a better agreement with micro-SDLA. This indicates that there is a significant influence of the microphysical scheme on the water vapour mixing ratios in the upper troposphere.

To test the importance of the horizontal resolution on the mesoscale model results two sensitivity tests were run. In the first one, we used a 50 km resolution (∼ECMWF horizontal resolution) in BRAMS instead of 20 km. The corresponding statistics that are given in Table 1 show that using a 50 km horizontal resolution leads to results very close to the reference simulation. The second sensitivity simulation was run with two nested grids. The outer grid is the reference run grid (20 km horizontal resolution) and the inner grid is centred on Bauru and has a 5 km horizontal resolution. For the 5 km grid, the convection parameterization is not used because the convection parametrization is not designed for a 5 km grid and the convection can possibly be explicitly represented with a 5 km grid. The statistics for this run are close to the reference run with a slight deterioration. The analysis of the two sensitivity runs shows the impact of the horizontal resolution is neutral. This indicates that, for this case study, the measured water vapour and temperature variations result mainly from the large scale dynamics rather than from local processes.

In summary, the mesoscale model performs better than ECMWF analysis in predicting the observed SF2 water vapour and RHI profiles when run with a similar resolution. With a 250 m vertical resolution, the BRAMS model is able to simulate most of the observed small scale vertical variations thanks to the fine vertical resolution and to a realistic representation of the microphysical processes. In this case, a fine vertical resolution is more important than a fine horizontal resolution because the observed variations of water vapour are mainly linked to the large scale dynamics.

4.4 Analysis of the reference run for SF2

In this section, we analyse the model results in order to identify the processes leading to the modelled temperature and humidity profiles and to understand the model behaviour compared to the observations. This study being focused on the UTLS we will restrict this analysis to the results above 10 km altitude. Within the UTLS (meaning here above 10 km) it is possible to identify the TTL (tropical tropopause layer) which is the transitional layer between air with tropospheric properties and air with stratospheric properties (Highwood and Hoskins, 1998; Folkins et al., 1999). The issue of how to define the TTL is not settled. Here, we define the top at the lapse rate tropopause (WMO definition) and the bottom where the lapse rate ($-\partial T/\partial z$) starts departing from typical tropospheric values (7–8 K km^{-1}) towards stratospheric values (negative values). Using this definition we found that the model predicts a TTL extending from 13.7 to 15.9 km. This result is compared to the TTL extension determined by Durry et al. (2006) from the SF2 micro-SDLA temperatures and the quasi-simultaneous ozone sounding measurements. They found using the chemopause for the bottom of the TLL and the lapse rate tropopause for the top that the observed TTL is between 13.5 and 15.5 km altitude. Thus, the TTL predicted by the model is in agreement within 0.4 km with micro-SDLA measurements. But the model does not provide the observed sharp temperature minimum around 15.5 km but a fairly smooth transition between the positive and the negative lapse rates.

A trajectory analysis is used to diagnose the processes that lead to the modelled water vapour and temperature profiles above 10 km altitude. Backward trajectories were calculated along the SF2 descent locations using the methodology proposed by Freitas et al. (2000). The trajectories are only reliable if the modelled convective precipitation is well located. This point is checked by comparing the TRMM accumulated rainrate (Fig. 2a) to the model accumulated rainrate (Fig. 2c). The comparison shows that, although the model simulates significantly less precipitation amount than observed, the spatial pattern of the model precipitation field agrees generally well with the TRMM observations. Only backward trajectories over 12 h are used since the analysis performed here is limited to the processes that occur just before the flight measurements.

Three layers are defined in this analysis: layer 1 corresponding to tropospheric air below the TTL base, layer 2 corresponding to the TTL and layer 3 corresponding to stratospheric air above the TTL top. The results of the trajectory analysis are given in Fig. 6 and summarized in Table 2. In layer 1 (10–13.7 km), the model predicts very accurately both temperature and RHI profiles except for the thin layer of supersaturated air observed in the 13.5–14 km altitude range (Fig. 5c). This particular layer will be discussed in more details below together with the analysis of layer 2. Between 10 and 12.8 km, the model results agree very well for the temperature and for r_v and thus for RHI. In this layer, the trajectory analysis indicates that the air is lifted by the front located south-west of Bauru and experiences the formation of large amounts of ice particles leading to a significant removal of water vapour (dehydration). This shows that the model is able to simulate well both the dynamical and the microphysical processes that lead to the observed r_v and T. To test the impact of the ice microphysical process on water vapour a

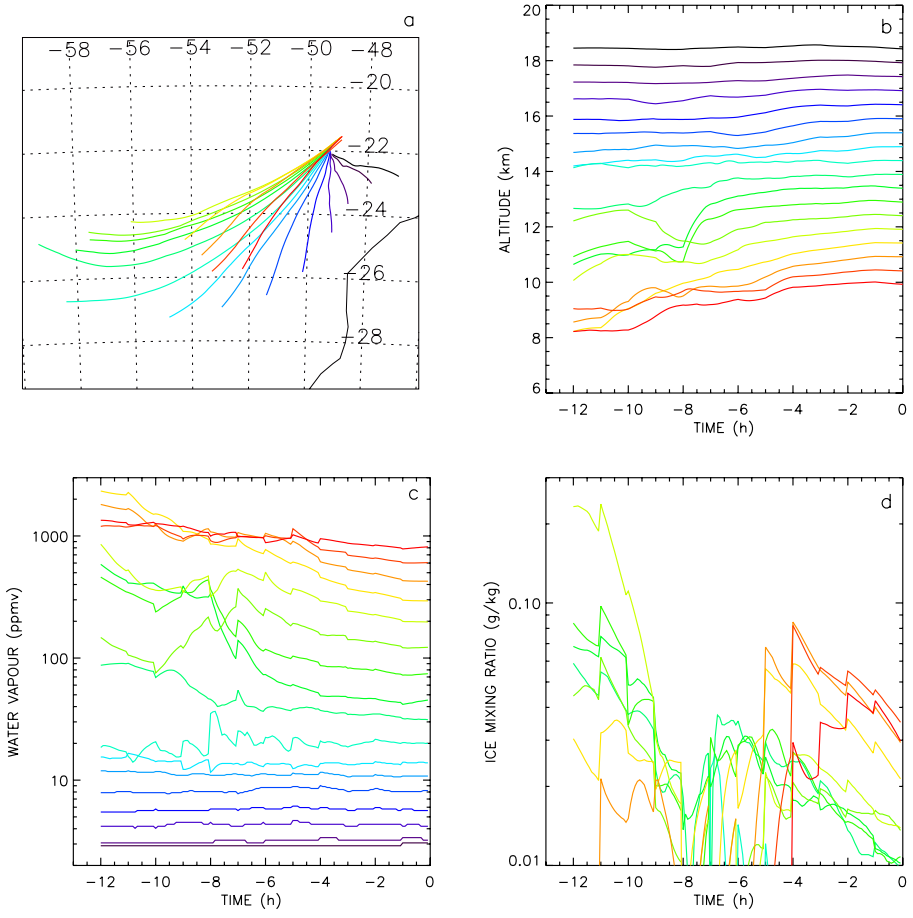

Fig. 6. Results from the 12-h backward trajectories calculated using the reference run results for SF2. **(a)** Map of the trajectories, **(b)** Altitude in km as a function of time in h, **(c)** water vapour mixing ratio in ppmv as a function of time in h and **(d)** ice (cloud+precipitation) mixing ratio in g kg^{-1} as a function of time in h.

Table 2. Characteristics of the three layers identified from the SF2 trajectory analysis based on the BRAMS reference simulation above 10 km altitude.

	Altitude range (km)	Air mass origin vert./horiz.	Moisture tendency	Ice condensation during previous hours
Layer 1	10–13.7	Mid and upper troposphere below the TTL/South-west	drying	yes
Layer 2 (TTL)	13.7–15.9	Upper troposphere below the TTL and TTL /South-west	drying below 14.3 km and constant above	yes only below 14.3 km
Layer 3	Above 15.9	Stratosphere/South changing to East with increasing altitude	constant	No

sensitivity simulation was run with simplified microphysics in which the water vapour can only be condensed as liquid cloud water where supersaturation with respect to liquid water occurs (i.e. no ice particles can be produced). For the sensitivity run displayed in Fig. 7, r_v mean profile in layer 1 is greater by about a factor of 1.4 on average compared to the reference run. This is confirmed by the statistical results given in Table 1. This large difference comes from the ice formation/growth and the consecutive dehydration by sedimentation which are not taken into account in the simplified

microphysics run. This indicates that it is necessary to include this process to obtain a realistic water vapour profile.

In layer 2 (TTL, 13.7–15.9 km), the trajectory analysis showed that the air slowly rises due to radiative warming except below 14.3 km where there is some formation of ice because of air ascent during the previous 12 h leading to dehydration. At the time of the flight, the 13.5–14.3 km layer in the model is still slightly supersaturated and the water vapour mixing ratio is nearly constant in the model during the 6 h preceding the flight. This quasi steady-state is explained by the fact that the decrease of r_v due to ice condensation leads to an increase of temperature through latent heat release which restricts the supersaturation and thus the decrease of r_v due to the ice formation. The large peaks of supersaturation observed around 13.5 km and around 15.5 km (Fig. 5c) are not reproduced by the model which produces too warm temperatures (Fig. 5b) at these altitudes. The water vapour field being linked to temperature conditions in particular when close to saturated conditions, it is important to evaluate the possible impact of the model temperature overestimation on the water vapour field. For this purpose, RHI was recalculated using the model r_v profile and the micro-SDLA temperatures instead of the model temperatures. The result displayed in Fig. 5c (green solid line) shows that if the BRAMS model had simulated more realistic temperatures in these two layers it would have lead to larger ice supersaturations and thus to a much better agreement with micro-SDLA RHI profile, particularly for the layer around 15.5 km altitude. This is also shown by the RHI RMSE calculated for the reference run but with the measured temperatures which is largely improved: 15.7%.

In the lower stratosphere (layer 3, above 15.9 km), the BRAMS model predicts a temperature consistent with the micro-SDLA measurements. The r_v profile is slightly moister below 17.2 km and largely drier above. The trajectory analysis shows that, in layer 3, there is no ice formation because the air does not experience saturated or supersaturated conditions during the past 12 h. Above 17.2 km, the model produces a stratospheric water vapour profile very close to the ECMWF analysis. This is because no small or meso-scale processes occur. Indeed, the water vapour distribution in this layer is mainly driven by the large scale horizontal fluxes since (i) vertical motions are weak and there is no convective overshooting in the BRAMS domain and (ii) no microphysical processes occur because air is largely undersaturated.

In summary, simulation results showed that the microphysical processes play an important role in the distribution of water vapour and an appropriate parameterization allowing supersaturation with respect to ice is needed to model the observed r_v profiles. In near saturated or supersaturated layers it is necessary to simulate realistic temperatures since microphysical processes are extremely temperature dependent.

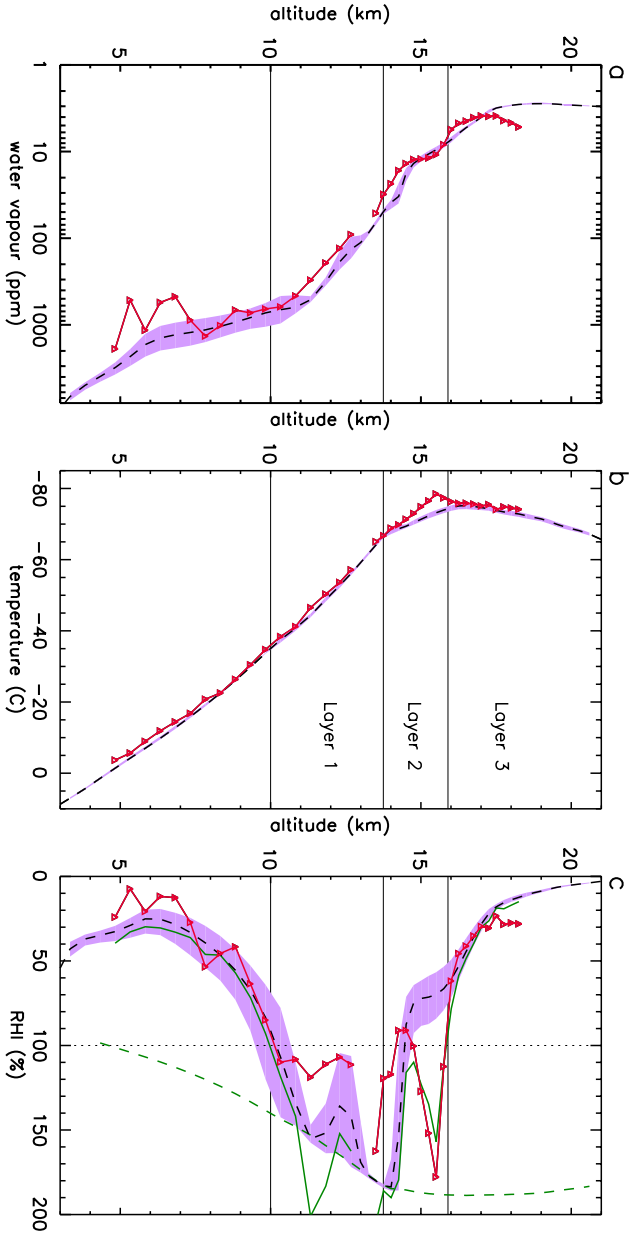

Fig. 7. Same as Fig. 5 but for the BRAMS sensitivity run with simplified microphysics (see text for details on this run).

5 Results for SF4 flight

5.1 SF4 flight and its meteorological environment

The SF4 balloon was launched from Bauru at 20:03 UTC on 24 February 2004. The balloon reached a maximum altitude of 20.2 km shortly before sunset followed by 45 min float and a slow descent (starting at 21:57 UTC) down to 10.7 km where it was cut down (00:17 UTC). The trajectory of the balloon is shown in Fig. 1.

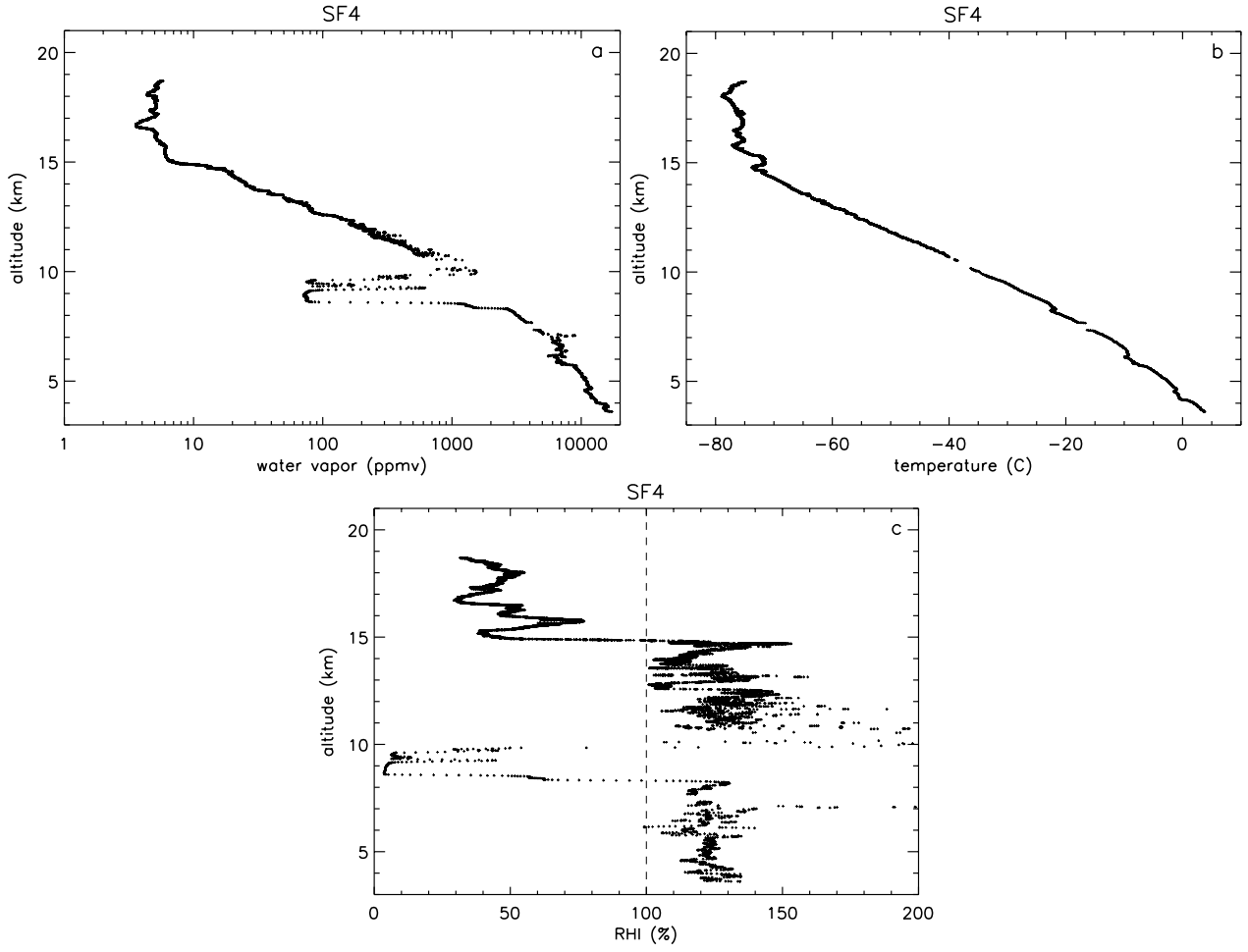

Fig. 8. Same as Fig. 3 but for SF4 flight measurements.

From noon onwards, a massive complex convective system was heading towards Bauru. At the time of the launch, the system was about 120 km north-west of Bauru, moving at 40 km h^{-1} south-eastwards. It reached Bauru shortly after 20:00 UTC. This system was part of a very large area of convection (SACZ; South Atlantic Convergence Zone) covering the State of São Paulo and extending over the ocean. The situation is illustrated in Fig. 2b by the accumulated TRMM rainfall between 24 February at 16:30 UTC and 25 February at 04:30 UTC. A more complete description of the meteorological situation is given in Durry et al. (2006).

5.2 SF4 water vapour and temperature profiles

For the SF4 flight analysis, we use H_2O data achieved during the descent of the sensor in the altitude region ranging from 18.7 km (24 February at 22:21 UTC) down to 3.6 km (25 February at 00:48 UTC). r_v, temperature and RHI profiles for the SF4 flight are shown in Fig. 8. One important feature in Fig. 8a is a very dry layer around 9 km with mixing ratios below 100 ppmv. The r_v profile also exhibits relative minima of water vapour around 15 km and 16.7 km altitude. The temperature profile decreases fairly monotonically up to 14.5 km altitude. Above there are significant variations with altitude with an absolute minimum of $-78.8°$C at 18.1 km. The measured profile is supersaturated up to 15 km altitude with the exception of the very dry layer between 8.5 and 10 km (see Fig. 8c). In this very dry layer, RHI reaches values below 10%. Typical supersaturations are around RHI=125% with peaks up to 195%. Note that the water vapour profiles and the temperature profiles above 15 km for the SF2 and SF4 flights are significantly different. This is related to the different meteorological conditions in which the two profiles were measured.

5.3 Comparison of the reference run and ECMWF analysis with SF4 measurements

For SF4, the comparison between micro-SDLA and the ECMWF analysis (resp. reference run) is displayed in Fig. 9

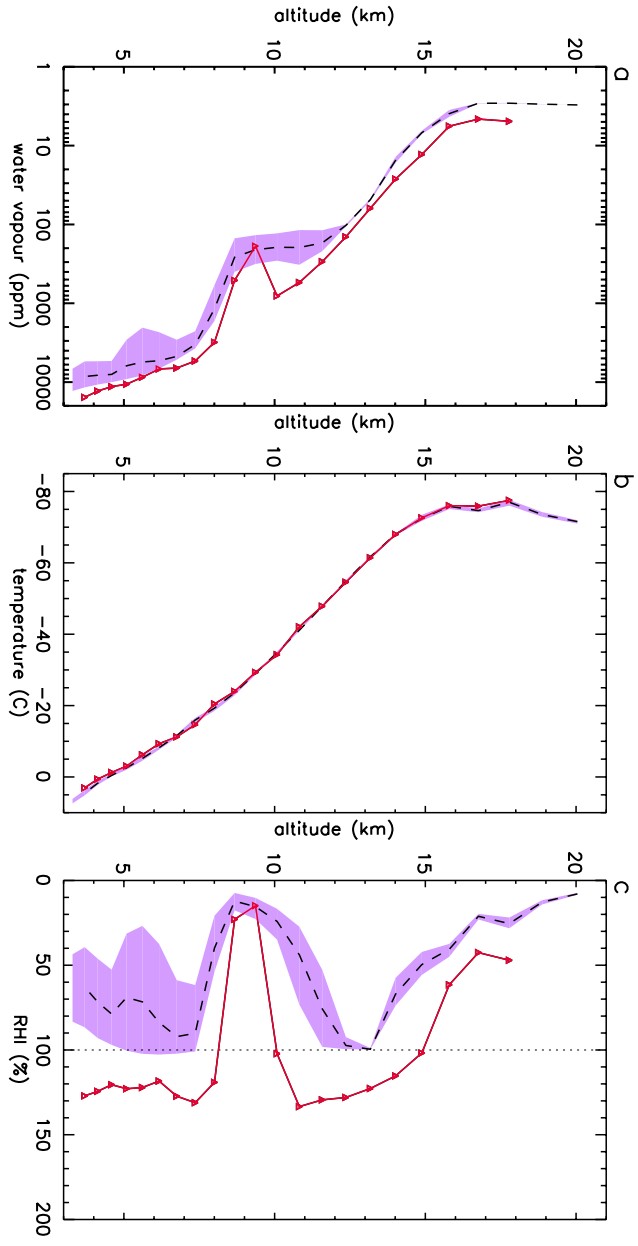

Fig. 9. Same as Fig. 4 but for SF4.

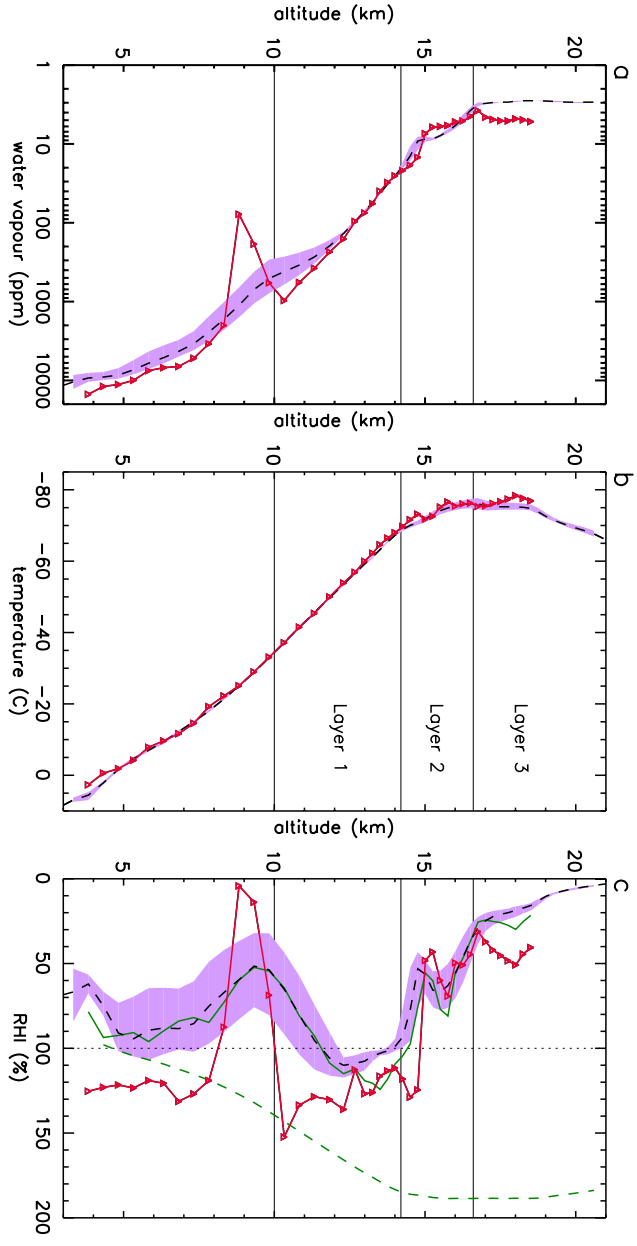

Fig. 10. Same as Fig. 5 but for SF4.

(resp. Fig. 10). We used ECMWF analysis at 00:00 UTC on 25 February 2004 and BRAMS hourly outputs from 22:00 UTC on 24 February 2004 to 01:00 UTC on 25 February 2004.

Figure 9a shows that ECMWF analysis r_v is generally dryer than the micro-SDLA r_v mean profile for all altitudes except in the very dry layer located around 9 km which is well captured by the ECMWF analysis. For temperature (Fig. 9b), the ECMWF analysis is consistent with the microSDLA measurements within 1 K. The ECMWF RHI profile (Fig. 9c) reproduces the general shape of the observations (RHI correlation=0.801) but is characterised by largely lower values (RMSE=48.5%) compared to microSDLA RHI except in the dry layer (see Table 3). There is hardly any supersaturation with respect to ice in the ECMWF analysis in the layers 3.5–8 km and 10–15 km. As for SF2, ECMWF analysis underestimates water vapour in the upper troposphere (above 10 km). This is partly because water vapour is immediately converted into ice when supersaturation with respect to ice occurs below −23°C. Another reason for the poor accuracy of ECMWF water vapour analysis in the UTLS is the few humidity data that are used in the assimilation system. Nevertheless, ECMWF analysis (14 February 00:00 UTC) is better than the 48 h forecast started on 12 February at 00:00 UTC as illustrated by the statistics given in Table 3.

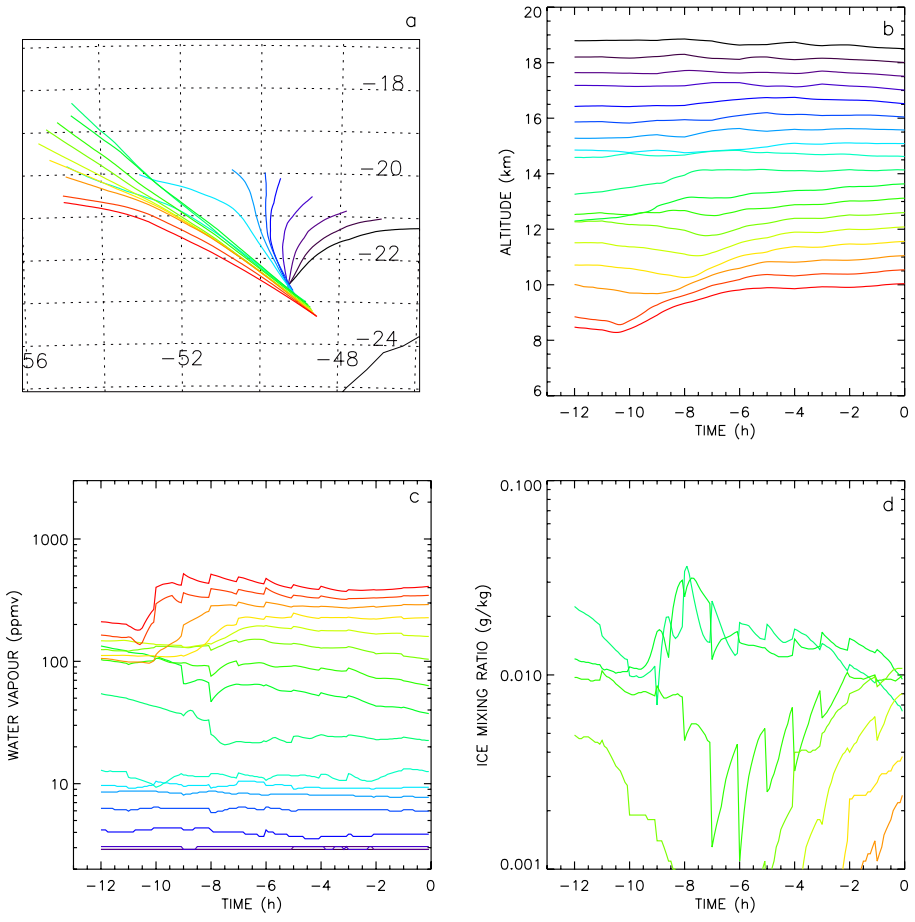

Fig. 11. Same as Fig. 6 but for SF4.

Table 3. Same as Table 1 but for SF4 flight.

	temperature RMSE (K)	RHI correlation	RHI RMSE (%)
ECMWF analysis	0.80	0.801	48.5
ECMWF 48 h forecast started on 23 Feb 2004 at 00:00 UTC	1.15	0.615	63.7
Run with 1 km vertical resolution	1.19	0.716	38.4
Reference run	1.26	0.778	33.9
Run with 50km horizontal resolution	1.29	0.769	35.1
Run with 5 km resolution (2 grids)	1.45	0.748	37.1
Run with simplified microphysics	1.63	0.499	54.9

As previously done for SF2, a sensitivity test with BRAMS was performed using a 1 km vertical resolution similar to the ECMWF model to allow a possible comparison to the ECMWF analysis. The corresponding results are given in Table 3. When using a 1 km vertical resolution, the BRAMS simulation RHI profile is significantly closer to the observations (RMSE=38.4%) than the ECMWF analysis (RMSE=48.5%). This is the contrary for temperature with values of RMSE of 1.19 K for the BRAMS and 0.80 K for ECMWF analysis. This means that for SF4, the ECMWF analysis is better for temperature compared to BRAMS with a similar vertical resolution. In Table 3 are also given the

statistics for the ECMWF 48 h forecast started on 23 February 2004, i.e. having the same initial state as the BRAMS simulations. Temperature RMSE for the ECMWF 48 h forecast is similar to the mesoscale simulation with 1km vertical resolution. This indicates that the good performance of the ECMWF analysis for temperature comes from the data assimilation. For RHI, the analysis statistics are poor but better than the 48h forecast statistics also thanks to data assimilation.

As shown in Figs. 10a and b, the main water vapour and temperature variations observed by micro-SDLA in the UTLS (TTL) are kept when averaged on the BRAMS reference run grid. The model profiles reproduce the general patterns found in the observations but they are smoother. In Fig. 10a, the mesoscale model produces a dry layer around 10 km altitude but significantly too moist compared to the micro-SDLA observations and the ECMWF analysis and located about 1 km higher. In the reference run, the SF4 flight track at the altitude of the dry layer is located in a transition zone associated with a large r_v gradient as illustrated by the large variability of the selected model profiles around the SF4 flight track in this layer. This transition zone is oriented north-west/south-east and located between the moist convection zone south of the transition zone and the dry intrusion of low stratosphere mid-latitude air ($\sim$100 ppmv) north of the transition zone as analysed by Durry et al. (2006). In the ECMWF analysis the SF4 flight track is located within the dry intrusion and gives more realistic results for the dry layer. This can be explained by the fact that for SF4: (i) the data assimilation has significantly decreased the water vapour mixing ratio in this layer and (2) the whole ECMWF analysis profile is significantly dryer than the observations. The comparison between the reference simulation and the microSDLA measurements indicates that the reference simulation forecasts the dry intrusion too far from the SF4 flight location, shifted by about 150 km. Below this layer, the reference run r_v profile is dryer than micro-SDLA. Above 12 km the model r_v is consistent with the measurements up to 16.8 km altitude. The micro-SDLA step-function shape is reproduced by the model although shifted in altitude by about 0.5 km. Above 16.8 km, the model is significantly dryer than the observations and exhibits very limited variations. Figure 10b shows that the temperature is well simulated in the reference run (RMSE=1.26 K) although the fine scale variations between 14.7 and 18 km are not produced by the model. For RHI (Fig. 10c), the model reproduces the general shape (RHI correlation=0.778) with generally significantly lower values (RMSE for RHI=33.9%).

The importance of the horizontal resolution is evaluated using two test simulations with 50 km and 5 km horizontal resolutions. Results of these sensitivity tests are fairly similar to the reference simulation as shown by the statistics given in Table 3. Similarly to SF2, there is no improvement possibly because the water vapour profile is mainly driven by the large scale dynamics.

In summary, the ECMWF analysis and the BRAMS simulations give good results for temperature and significantly underestimate on average RHI although the BRAMS model performs better. Compared to SF2, SF4 statistical results are slightly better for temperature ($\sim$1.2 K RMSE for SF4 and $\sim$1.7 K for SF2) but worse for RHI ($\sim$35% RMSE for SF4 and $\sim$25% for SF2) and consequently for r_v. This indicates that the BRAMS water vapour performance depends on the considered meteorological situation.

5.4 Analysis of the reference run for SF4

In this section we analyse in more details the BRAMS model behaviour compared to observations in the UTLS (above 10 km). The TTL base and top altitudes derived from the reference run are 14.2 and 16.6 km. The TTL characteristics derived from micro-SDLA data by Durry et al. (2006) are 13.3 km for the base and 17.8 km for the top. Therefore, the model predicts a TTL thinner than observed. In the micro-SDLA observations, there is a layer between $\sim$16.8 and $\sim$17.7 km altitude where the water mixing ratio is high ($\sim$5 ppmv) and the temperature tendency is negative. From the analysis of complementary ozone and CH_4 data, Durry et al. (2006) suggested that this layer had been moistened and cooled adiabatically by a convective transport that had occurred a few days before the flight. This moist and cold layer is not captured by the model leading to a TTL top at a lower altitude in the model. The 0.9 km difference between the TTL base observed and modelled may be attributed to the TTL base definitions used: the chemopause for the observations and the lapse rate for the model.

As for SF2, 12-h backward trajectories were calculated from the reference run outputs at the location of the SF4 flight. The modelled precipitation (Fig. 2d) is less in amount than the satellite observations but it is well located as illustrated by the comparison with TRMM accumulated rainrate (Fig. 2b). The results of the trajectory calculation are shown in Fig. 11 and summarized in Table 4. As for SF2, we define three layers: layer 1 below the TTL (10–14.2 km), layer 2 being the TTL (14.2–16.6 km) and layer 3 being the lower stratosphere (above 16.6 km). In layer 1 (10–14.2 km), the reference run r_v and RHI are underestimated by the model mainly below 11km. The 10–11 km layer is the transition between the very dry layer and a moist layer. The model fails to reproduce the observed very sharp transition related to the intrusion of stratospheric extratropical air which started a few days before the flight. This intrusion has likely been smoothed during the two preceding days in the model by the turbulent mixing parametrization. This hypothesis is supported by the calculation of r_v integrated over the layer where the model predicts the dry intrusion (8.3 and 11.3 km) giving a 5% difference between micro-SDLA and the model results. This means that there is approximately the same amount of water vapour in the dry intrusion layer in the observations and in the model but it is more diluted in the model. The air

Table 4. Same as Table 2 but for SF4.

	Altitude range (km)	Air mass origin vertical/horizontal	Moisture tendency	Ice condensation during previous hours
Layer 1	10–14.2	Mid and upper troposphere below the TTL/North-west	Moistening below 12.6 km and drying above	Yes above 11 km and increasing with altitude
Layer 2 (TTL)	14.2–16.6	TTL/North-west changing to North with increasing altitude	Constant	No
Layer 3	Above 16.6	Stratosphere/North changing to East with increasing altitude	Constant	No

mass sampled by SF4 in layer 1 comes from ascending air from lower levels leading to a moistening during the hours preceding the flight. This moistening effect related to the dynamics competes with the removal of water vapour by ice nucleation and subsequent ice growth and sedimentation. This microphysical process becomes dominant in the model above 12.6 km leading to a net decrease of water vapour mixing ratio. The analysis of the SF2 flight showed that the temperature errors in the BRAMS simulation have an impact on the model's ability to reproduce the water vapour observations. For SF4, the temperature error is weaker (Fig. 10b and Table 3) and its impact is only important in the 12.5–14.7 km layer as illustrated in Fig. 10c (green solid line). In this layer, using the micro-SDLA temperature measurements and the BRAMS r_v to calculate RHI leads to an increase of RHI consistent with the observations. This result shows that part of the RHI underestimation in layer 1 is due to temperature errors in the model. The complementary possible explanations are an insufficient moistening of this layer by air ascent and/or a too fast drying by ice formation.

In layer 2 (TTL, 14.2–16.6 km), the water vapour does not exhibit significant changes during the preceding hours since it does not experience significant uplifting or ice formation because of undersaturated conditions. The distribution of water vapour in the TTL depends on the dynamics. Below 15.2 km the trajectory analysis shows that the air originates from a relatively dry area located north-west of the flight track. In the 14.2–15.2 km layer, the BRAMS model is able to reproduce the observed shape and values for r_v and RHI. Between 15.2 and 16.6 km the air comes from the convective area north of Bauru. This air is undersaturated within the 12 h preceding the flight but it is more humid in terms of relative humidity than below because previously moistened by convection (see Figs. 2b and d). This effect becomes less important above 16 km altitude leading to the decrease of the BRAMS RHI between 16 and 16.6 km. Nevertheless, the BRAMS model is able to simulate the observed variations of r_v and RHI between 14.2 and 16.6 km meaning that the model dynamics is realistic and in particular the location of the convection. Above 16.6 km in the lower stratosphere (layer 3), the model water vapour variations are small leading to a negligible impact of the horizontal dynamics on the water vapour distribution. As for SF2, the BRAMS model initial state for r_v is fairly homogeneous above 17 km. The r_v field is not changed during the simulation since this layer is not affected by any air ascent or ice nucleation.

6 Conclusion

The objective of this paper is to evaluate the ability of the BRAMS mesoscale model to simulate the observed vertical variations of water vapour in the tropical UTLS. This evaluation is based on comparisons with in situ water vapour and temperature measurements but also comparisons with ECMWF analysis fields in order to show the potential benefits of a mesoscale model with respect to a global analysis. The water vapour and temperature measurements were gathered by the micro-SDLA instrument during the SF2 and SF4 HIBISCUS balloon flights. Both flights exhibit large variations of water vapour in the UTLS but also large differences are found between the two sets of measurements. In both flights, layers with large supersaturations with respect to ice are observed.

The measured fine scale vertical structures in the UTLS have a typical length of 1 km or less. This is why a 250 m vertical grid-spacing was used in the UTLS in the BRAMS. The ECMWF model having a ∼1 km vertical grid-spacing in the UTLS can only give a smooth picture of the observed variations of temperature and water vapour. Apart from the vertical resolution, the differences between the BRAMS reference simulation and the ECMWF analysis are:

– the horizontal resolution: 20 km for BRAMS and ∼50 km for ECMWF,

– a more complete microphysical scheme in BRAMS giving the possibility of large supersaturations with respect to ice,

– the assimilation of data in the ECMWF analysis when available giving the possibility to take into account

valuable recent meteorological information leading to an update of the atmospheric state compared to any forecast (from BRAMS or ECMWF).

Sensitivity simulations with BRAMS were run to evaluate the impact of the vertical resolution, horizontal resolution and microphysical scheme on the mesoscale model performances.

The analysis of the results showed that the ECMWF analysis performs well compared to the micro-SDLA measurements for temperature for both flights. This is related to the data assimilation system which improves significantly the temperature field. As already found in previous studies (e.g. Ovarlez et al., 2000), we showed that ECMWF analysis generally underestimates water vapour in the upper troposphere. In supersaturated layers, we pointed out that the microphysical scheme removes instantaneously the excess of water vapour with respect to ice leading to lower water vapour mixing ratios compared to observations. Very recently, Tompkins et al. (2005) tested a new parameterization that attempts to represent ice supersaturation and the homogeneous ice nucleation process in the ECMWF model. They showed that this new parameterization leads to a reduction of the upper troposphere dry bias. In undersaturated conditions below 10 km altitude, ECMWF analysis reproduces generally well micro-SDLA water vapour profile. This is because water vapour information from radiosoundings below 10 km is used in the assimilation system. This is also because in undersaturated conditions the water vapour distribution does not rely on the microphysics but depends on the dynamics that is also well constrained by data assimilation. Above 17 km altitude, ECMWF analysis is drier than micro-SDLA for both flights.

The mesoscale simulation with the BRAMS model provides a generally good estimation of the measured temperature profiles except in layers with large gradients or with small scale variations of the gradient which are not well captured. In particular, this leads to a difference of $\sim$5 K at the cold point tropopause between micro-SDLA and BRAMS for SF2. For SF4, the BRAMS statistical results for temperature are slightly worse than the ECMWF analysis but similar to the ECMWF 48 h forecast.

For water vapour and RHI (relative humidity with respect to ice saturation), the BRAMS model with a 1 km vertical resolution gives significantly better results than the ECMWF analysis with a reduction of the RHI RMSE of about 10% in both cases. This improvement is mainly due to the microphysical scheme in BRAMS which can give ice supersaturations and a progressive removal of water vapour by ice nucleation and subsequent growth and sedimentation. The mesoscale simulation with a 250 m vertical resolution is able to reproduce most of the observed vertical variations of water vapour and of RHI. Neverthess, it does not exhibit very large ice supersaturations (max RHI $\sim$130%) like those found in the micro-SDLA data (max RHI$>$150%). This can be explained by the fact that (i) measured highest supersaturations are likely to be a transient state just before ice nucleation occurs and (ii) the BRAMS microphysical scheme is a bulk type parameterization which is less precise than a spectral bin parameterization for thin cirrus simulation as shown by Khvorostyanov et al. (2006). The impact of the horizontal resolution is small for both case studies. Above 17 km altitude, the underestimation of water vapour by BRAMS is similar to the ECMWF analysis since no mesoscale process affects the lower stratosphere in the BRAMS simulations.

From a trajectory analysis, it was shown that the water vapour variations in the model depend on the dynamical and thermodynamic processes experienced by the sampled air parcel. The profiles from two flights undergo a range of different dynamical processes: uplifting from the mid troposphere, large scale transport associated with a front, isentropic transport from the mid-latitude upper troposphere and convection. The dynamical processes are dominant in undersaturated conditions. In near-saturated or supersaturated conditions the thermodynamic environment, i.e. the air temperature, plays a major role since it controls the ice nucleation process and consequently the dehydration. For instance, the sharp minimum of temperature at the cold point tropopause in SF2 is not captured by the model leading to a large underestimation of RHI. In supersaturated layers where the BRAMS temperature is close to micro-SDLA, the model water vapour profile is generally close to the observations showing the good quality of the model's microphysical parameterization. The origin of the temperature uncertainties found in the BRAMS simulations and the ECMWF forecasts were not investigated in the present study. Temperature being dependent on many processes (radiative, dynamic, thermodynamic and microphysical), a special work needs to be done on this issue.

The BRAMS mesoscale model is able to reproduce most of the vertical variations of water vapour in the UTLS. But the two cases studied in this paper are not sufficient to fully evaluate the mesoscale model performances to simulate the UTLS water vapour. In particular, since only one measured profile was available per case study, it was not possible to follow the time evolution of the water vapour structures. This knowledge of the time evolution would help confirming our interpretation of the processes involved in the variations of water vapour. A larger set of data was acquired during the SCOUT-AMMA field experiment that took place in western Africa in 2006. This will give the opportunity to obtain a more complete description from observations of the time evolution of the dynamical, thermodynamic and microphysical processes driving the UTLS water vapour. Also the availability of more accurate water vapour sensors in radiosounding systems will be a determinant tool in the understanding of the water vapour evolution in the UTLS.

Acknowledgements. This modelling study is supported by funds from the European Commission 5th PCRD (HIBISCUS project;

contract EVK2-2001-000111) and the French Centre National de la Recherche Scientifique (Programme National de Chimie Atmosphérique). This work makes use of the RAMS model, which was developed under the support of the National Science Foundation (NSF) and the Army Research Office (ARO). BRAMS model development and maintenance is supported by Brazilian Funding Agency for Studies and Projects (FINEP). Computer ressources were provided by CINES (Centre Informatique National de l'Enseignement Supérieur), project pce2227. The TRMM data were provided by GSFC/DAAC, NASA. The authors thank the coordinators of the TroCCiBras Project and the personnel of the Meteorological Research Institute (IPMet) of the São Paulo State University (UNESP) for providing the infrastructure support during the campaign and the personnel of the Centre National d'Etudes Spatiales (CNES) for their support in balloon, radar and sondes operations. We acknowledge G. Held of IPMet for providing the Bauru radar observations and assisting with their interpretation.

Edited by: P. Haynes

References

Brewer, A. W.: Evidence for a world circulation provided by measurements of helium and water vapour distribution in the stratosphere, Quart. J. Roy. Meteorol. Soc., 75, 351–363, 1949.

Durry, G. and Mégie, G.: Atmospheric CH_4 and H_2O monitoring with near-infrared InGaAs laser diodes by the SDLA, a balloonborne spectrometer for tropospheric and stratospheric in situ measurements, Appl. Opt., 38, 7342–7354, 1999.

Durry, G. and Megie, G. : In situ measurements of H_2O from a stratospheric balloon by diode laser direct-differential absorption spectroscopy at 1.39 μm, Appl. Opt., 39, 5601–5608, 2000.

Durry, G., Hauchecorne, A., Ovarlez, J., Ovarlez, H., Pouchet, I., Zeninari, V., and Parvitte, B.: In situ measurement of H_2O and CH_4 with telecommunication laser diodes in the lower stratosphere: dehydration and indication of a tropical air intrusion at mid-latitudes, J. Atmos. Chem., 43, 175–194, 2002.

Durry, G., Amarouche, N., Zéninari, V., Parvitte, B., Le Barbu, T., and Ovarlez, J.: In situ sensing of the middle atmosphere with balloonborne near-infrared laser diodes, Spectrochimica Acta, Part A, 60, 3371–3379, 2004.

Durry, G. and Hauchecorne, A.: Evidence for long-lived polar vortex air in the mid-latitude summer stratosphere from in situ laser diode CH_4 and H_2O measurements, Atmos. Chem. Phys., 5, 1467–1472, 2005, http://www.atmos-chem-phys.net/5/1467/2005/.

Durry, G., Zeninari, V., Parvitte, B., Le Barbu, T., Lefevre, F., Ovarlez, J., and Gamache, R. R.: Pressure-broadening coefficients and line strengths of H_2O near 1.39 μm: application to the in situ sensing of the middle atmosphere with balloonborne diode lasers, J. Quant. Spectrosc. Radiat. Trans., 94(3–4), 387–403, 2005.

Durry, G., Huret, N., Hauchecorne, A., et al.: Isentropic advection and convective lifting of water vapor in the UT-LS as observed over Brazil (22° S) in February 2004 by in situ high resolution measurements of H2O, CH4, O3 and temperature, Atmos. Chem. Phys. Discuss., 6, 12 469–12 501, 2006.

Flatau, P. J., Walko, R. L., and Cotton, W. R.: Polynomial fits to saturation vapour pressure, J. Appl. Meterorol., 31, 1507–1513, 1992.

Folkins, I., Loewenstein, M., Podolske, J., Oltmans, S., and Proffitt, M.: A barrier to vertical mixing at 14 km in the tropics: Evidence from ozonesondes and aircraft measurements, J. Geophys. Res., 104, 22 095–22 102, 1999.

Fouquart, Y. and Bonnel, B., Computations of solar heating of the earth's atmosphere: a new parametrization, Breitr. Phus. Atmosph., 53, 35–62, 1980.

Freitas, S. R., Silva Dias, M. A. F., Silva Dias, P. L., Longo, K. M., Artaxo, P., Andreae, M. O., and Fischer, H.: A convective kinematic trajectory technique for low-resolution atmospheric models, J. Geophys. Res., 105, 24 375–24 386, 2000.

Freitas, S., Longo, K., Silva Dias, M., Silva Dias, P., Chatfield, R., Prins, E., Artaxo, P., Grell G., and Recuero, F.: Monitoring the transport of biomass burning emissions in South America. Environmental Fluid Mechanics, 5(1–2), 135–167, doi:10.1007/s10652-005-0243-7, 2005.

Fueglistaler, S., Wernli, H., and Peter, T.: Tropical troposphere-to-stratosphere exchange inferred from trajectory calculations, J. Geophys. Res., 109, D03108, doi:10.1029/2003JD004069, 2004.

Fujiwara, M., Shiotani, M., Hasebe, F., Vömel, H., Oltmans, S., Ruppert, P. W., Horinouchi, T., and Tsuda T.: Performance of the meteolabor "Snow White" chilled-mirror hygrometer in the tropical troposphere: Comparisons with the Vaisala RS80 A/H-Humicap sensors, J. Atmos. Ocean. Technol., 20, 1534–1542, 2003.

Gettelman, A., Randel, W. J., Wu, F., and Massie, S. T.: Transport of water vapour in the tropical tropopause layer, Geophys. Res. Lett., 29, 1009, doi:10.1029/2001GL013818, 2002.

Gevaerd, R. and Freitas, S.: Estimativa operacional da umidade do solo para iniciao de modelos de previso numrica da atmosfera. Parte 1: descrio da metodologia e validao, Brazilian J. Meteorol., LBA Special Issue, 21, 3a, 59–73, 2006.

Grell, G. A. and Devenyi, D.: A generalized approach to parameterizing convection combining ensemble and data assimilation techniques, Geophys. Res. Lett., 29, 1693, doi:10.1029/2002GL015311, 2002.

Harrington, J. Y.: The effects of radiative and microphysical processes on simulated warm and transition season Arctic stratus, PhD Diss., Atmospheric Science Paper No. 637, Colorado State University, Department of Atmospheric Science, Fort Collins, CO 80523, 289 pp, 1997.

Hatsushika, H. and Yamazaki, K.: Stratospheric drain over Indonesia and dehydration within the tropical tropopause layer diagnosed by air parcel trajectories, J. Geophys., Res., 108, D4610, doi:10.1029/2002D002986, 2003.

Highwood, E. J. and Hoskins, B. J.: The tropical tropopause, Quart. J. Roy. Meteorol. Soc., 124, 1579–1604, 1998.

Hintsa, E., Weinstock, E. M., Anderson, J. G., May, R. D., and Hurst, D. F.: On the accuracy of in situ water vapour measurements in the troposphere and lower stratosphere with the Harvard Lyman-a hygrometer, J. Geophys. Res., 104, 8183–8190, 1999.

Holton, J. R., Haynes, P. H., McIntyre, M. E., Douglass, A. R., Tood, R. B., and Pfster, L.: Stratosphere-troposphere exchange, Rev. Geophys., 105, 1879–1888, 1995.

Jensen, E. and Pfister, L.:Transport and freeze-drying in the tropical tropopause layer, J. Geophys. Res., 108, D02207, doi:10.1029/2003JD004022, 2004.

Jensen, E., Pfister, L., Bui, T., Weinheimer, A., Weinstock, E.,

Smith, J., Pittman, J., Baumgardner, D., Lawson, P., and McGill, J.: Formation of a tropopause cirrus layer observed over Florida during CRYSTAL-FACE, J. Geophys. Res., 110, D03208, doi:10.1029/2004JD004671, 2005a.

Jensen, E., Smith, J., Pfister, L., Pittman, J. L., Weinstock, E., Sayres, D. S., Herman, R. L., Troy, R. F., Rosenlof, K., Thompson, T. L., Fridlind, A. M., Hudson, P. K., Cziczo, D. J., Heysfield, A. J., Schmitt, C., and Wilson, J. C.: Ice supersaturations exceeding 100% at the cold tropical tropopause: implications for cirrus formation and dehydration, Atmos. Chem. Phys., 5, 851–862, 2005b.

Khvorostyanov, V. I., Morrison, H., Curry, J. A., Baumgardner, D., and Lawson, P.: High supersaturation and modes of ice nucleation in thin tropopause cirrus: Simulation of the 13 July 2002 Cirrus Regional Study of Tropical Anvils and Cirrus Layers case, J. Geophys. Res., 111, D02201, doi:10.1029/2004JD005235, 2006.

May, R. D.: Open path near-infrared tunable diode laser spectrometer for atmospheric measurements of H_2O, J. Geophys. Res., 103, 19 161–19 172, 1998.

Mellor, G. L. and Yamada, T.: Development of a turbulence closure model for geophysical fluid problems, Rev. Geophys. Space Phys., 20, 851–875, 1982.

Miloshevich, L. M., Vömel, H., Paukkunen, A., Heymsfield, A. J., and Oltmans, S. J.: Characterization and correction of relative humidity measurements from Vaisala RS-80-A radiosondes at cold temperatures, J. Atmos. Ocean. Technol., 18, 135–156, 2001.

Mlawer, E. J., Taubman, S. J., Brown, P. D., Iacono, M. J., and Clough, S.A.: Radiative transfer for inhomogeneous atmospheres: RRTM, a validated correlated-k model for the longwave, J. Geophys. Res., 102D, 16 663–16 682, 1997.

Morcrette, J.-J.: Revision of the clear-sky and cloud radiative properties in the ECMWF model, ECMWF newsletter, 61, 3–14, 1993.

Morcrette, J.-J., Clough, S. A., Mlawer, E. J., and Iacono, M. J.: Impact of a validated radiative transfer scheme, RRTM, on the ECMWF model climate and 10-day forecasts, ECMWF Technical Memo., No. 252, 47 pp, 1998.

Offermann, D., Schaeler, B., Riese, M., Langfermann, M., Jarisch, M., Eidmann, G., Schiller, C., Smit, H. G. J., and Read, W. G.: Water vapor at the tropopause during the CRISTA 2 mission, J. Geophys. Res., 107(D23), 8176, doi:10.1029/2001JD000700,2002.

Ovarlez, J. and Van Velthoven, P.: Comparison of water vapour measurements with data retrieved from ECMWF analyses during the POLINAT experiment, J. Appl. Meteorol., 36, 1329–1335, 1997.

Ovarlez, J., Van Velthoven, P., Sachse, G., Vay, S., Schlager, H., and Ovarlez, H.: Comparison of water vapour measurements from POLINAT 2 with ECMWF analyses in high-humidity conditions, J. Geophys. Res., 105, 3737–3744, 2000.

Ovarlez, J., Gayet, J.-F., Gierens, K, Ström, J., Ovarlez, H., Auriol, F., Busen., R., and Schumann, U.: Water vapour measurements inside cirrus clouds in northern and southern hemispheres during INCA, Geophys. Res. Lett., 29, 1813, doi:10.1029/2001GL014440, 2002.

Parvitte B., Zeninari, V., Pouchet, I., and Durry, G.: Diode laser spectroscopy of H_2O in the 7165–7185 cm^{-1} range for atmospheric applications, J. Quant. Spectros. Radiat. Trans., 75, 493–507, 2002.

Pommereau, J.-P., Garnier, A., Held, G., et al.: An overview of the HIBISCUS campaign, Atmos. Chem. Phys. Discuss., 7, 2389–2475, 2007, http://www.atmos-chem-phys-discuss.net/7/2389/2007/.

Sonntag, D.: The history of formulations and measurements of ice pressure, In proceedings of the 3rd Int. Symposium on Humidity and Moisture, National Physical Laboratory, UK, 93–102, 1998.

Spichtinger, P., Gierens, K., and Wernli, H.: A case study on the formation and evolution of ice supersaturation in the vicinity of a warm conveyor belt's outflow region, Atmos. Chem. Phys., 5, 973–987, 2005, http://www.atmos-chem-phys.net/5/973/2005/.

Tompkins, A. M., Gierens, K., and Rädel, G.: Ice supersaturation in the ECMWF Integrated Forecast System, ECMWF Technical Memorandum, 481, 2005.

Turner, D. D., Lesht, B. M., Clough, S. A.,. Liljegren, J. C., Revercomb, H. E., and Tobin, D. C.: Dry bias and variability in Vaisala RS80-H Radiosondes: The ARM experience, J. Atmos. Ocean. Technol., 20, 117–132, 2003.

Vömel, H., Oltmans, S. J., Johnson, B. J., Hasebe, F., Shiotani, M., Fujiwara, M., Nishi, N., Agama, M., Cornejo, J., Paredes, F., and Enriquez, H.: Balloon-borne observations of water vapor and ozone in the tropical upper troposphere and lower stratosphere, J. Geophys. Res., 107(D14), 4210, doi:10.1029/2001JD000707, 2002.

Walko, R. L., Cotton, W. R., Meyers, M. P., and Harrington, J. Y.: New RAMS cloud microphysics parameterization. Part I: the single-moment scheme, Atmos. Res., 38, 29–62, 1995.

Walko, R., Band, L., Baron J., Kittel, F., Lammers, R., Lee, T., Ojima, D., Pielke, R., Taylor, C., Tague, C., Tremback, C., and Vidale, P.: Coupled atmosphere-biophysics-hydrology models for environmental modeling, J. Appl. Meteorol. 39(6), 931–944, 2000.

Zöger, M., Afchine, A., Eicke, N., Gerhards, M. T., Klein, E., McKenna, D. S., Mörschel, U., Schmidt, U., Tan, V., Tuitjet, F., Woyke, T., and Schiller, C.: Fast in situ stratospheric hygrometers: A new family of balloonborne and airborne Lyman-alpha photofragment fluorescence hygrometers, J. Geophys. Res., 104, 1807–1816, 1999.